Y-12

Y/DZ-1190

OAK RIDGE Y-12 PLANT

MARTIN MARIETTA

THE USE OF FRACTALLYDESIGNED WAVEFORMS IN ELECTROFORMING

J. S. Bullock
R. L. Lawson
Lockheed Martin Energy Systems, Inc.

J. R. Kirkpatrick
Lockheed Martin Energy Research, Inc.

March 1, 1996

For submission to
American Electroplating and
Surface Finishing Society
for inclusion in conference proceddings of
AESF SUR/FIN 96 in Cleveland, OH
June 10-13, 1996

MANAGED BY
MARTIN MARIETTA ENERGY SYSTEMS, INC.
FOR THE UNITED STATES
DEPARTMENT OF ENERGY

Y/DZ-1190

THE USE OF FRACTALLY-DESIGNED WAVEFORMS IN ELECTROFORMING

J. S. Bullock
R. L. Lawson
Lockheed Martin Energy Systems, Inc.*

J. R. Kirkpatrick
Lockheed Martin Energy Research, Inc.

March 1996

*Managed by Lockheed Martin Energy Systems, Inc., under contract DE-AC05-84OR21400 with the U.S. Department of Energy

HH

DISCLAIMER

The Use of Fractally-Designed Waveforms in Electroforming

Jonathan S. Bullock and Roger L. Lawson
Lockheed Martin Energy Systems, Inc.

John R. Kirkpatrick
Lockheed Martin Energy Research, Inc.

Oak Ridge, TN 37831

Pulsed electrodeposition offers the potential for superior control of deposit properties because of the additional control variables available. However, the optimization of pulsed deposition processes is a challenge because of the complexity created by these additional variables. For example, the tendency of electroforms to acquire irregularities such as dendritic growths or other morphological instabilities, creates the need for methods to control these undesirable phenomena. One such method is periodic reverse pulses. The optimization of periodic reverse processes is not simple, and can lead to local solutions that do not optimize all properties simultaneously. One method for global optimization that might, for example, control surface irregularities on several size scales, uses a periodic reverse design based on a fractal time series. This incorporates deplating pulses of several lengths within one self-similar waveform. The properties of fractals permit the control of highly complex designs with a small number of input variables. The creation of such waveforms, their properties, and their use in a lead-plating process are described. Speculation on the potential for further application of this method is offered.

Introduction

Definition and Rationale

The current state of the art in pulsed plating is well described in the book edited by Puippe and Leaman[1]. Fractally-designed waveforms are a special class of pulsed, periodic reverse electroforming waveforms. This waveform class is actually a superset of the usual type of pulsed, periodic reverse waveforms, as the usual type exists as a subset of this fractal class.

For this paper, fractal electroforming waveforms are pulsed waveforms incorporating both cathodic (plating) pulses with a given duty cycle, and also anodic (deplating) pulses with more than one time scale. These are distributed through the waveform such that they form a self-similar (i.e., fractal) pattern in time.Using anodic pulses of several time scales might permit controlling surface irregularities on several size scales. The structure of these time scales can be tailored to the specific plating system. A reference to the level of the fractal waveform describes the number of time scales on which anodic pulses appear. As will be explained in the Experimental section, these waveforms are generated using methods that are straightforward, although they are not commonly used in plating practice.

Figure 1 shows in symbolic notation the pattern of pulses and off-times that make up a 4-level fractal waveform. The P_c element is the cathodic pulse. It is repeated n_c times, and then the zeroth-level anodic pulse P_{a0} is applied. This combined pulse train is repeated n_0 times, then a first-level anodic pulse P_{a1} is applied and this combined pulse train is repeated n_1 times, and so on. The self-similarity of these waveforms is in general related to the total quantity of current passed; for example, the zeroth-level anodic pulse is intended to remove some fraction of the material deposited by the n_c cathodic pulses, the 1st-level anodic pulse removes that same fraction of material deposited during the n_0 combined pulse trains, and so on. If the same fraction is removed at each of n levels, the net fraction F_{net} of coulombs for the whole waveform is obtained as:

$$F_{net} = \left(\frac{C_c^{nth} - C_a^{nth}}{C_c^{nth}}\right)^n = \frac{C_c^{net}}{C_c^{tot}}$$

Figure 2 illustrates the first two levels of a multilevel fractal waveform. Nine cathodic pulses are followed by one anodic pulse; this train repeats 9 times, then is followed by a longer anodic pulse. For a 3-level fractal, this combined train would repeat n times and would be followed by an even longer pulse, and so on.

Designs Used

The cathodic pulses are typically short and of rectangular profile; for this study, durations of 1 ms were typically used. Anodic pulses for this study were typically (to use a 4-level fractal example): 2X, 20X, 200X and 2000X the length of the cathodic pulse for the respective levels. This assumes a rectangular pulse shape, and the pulse duration of triangular and trapezoidal pulses would be correspondingly longer to keep the coulomb ratio to scale. Anodic pulse amplitudes were about the same as the cathodic pulses, give or take a factor of two. A typical cathodic pulse current density was about 1.05 A cm^{-2}.

$$(((((P_c + off)_{n_c} + P_{a_0} + off)_{n_0} + P_{a_1} + off)_{n_1} + P_{a_2} + off)_{n_2} + P_{a_3} + off)_{n_{tot}}$$

Figure 1 - Symbolic notation describing the structure of a 4-level fractal waveform which has arbitrary amplitudes and arbitrary numbers of repeats at each level

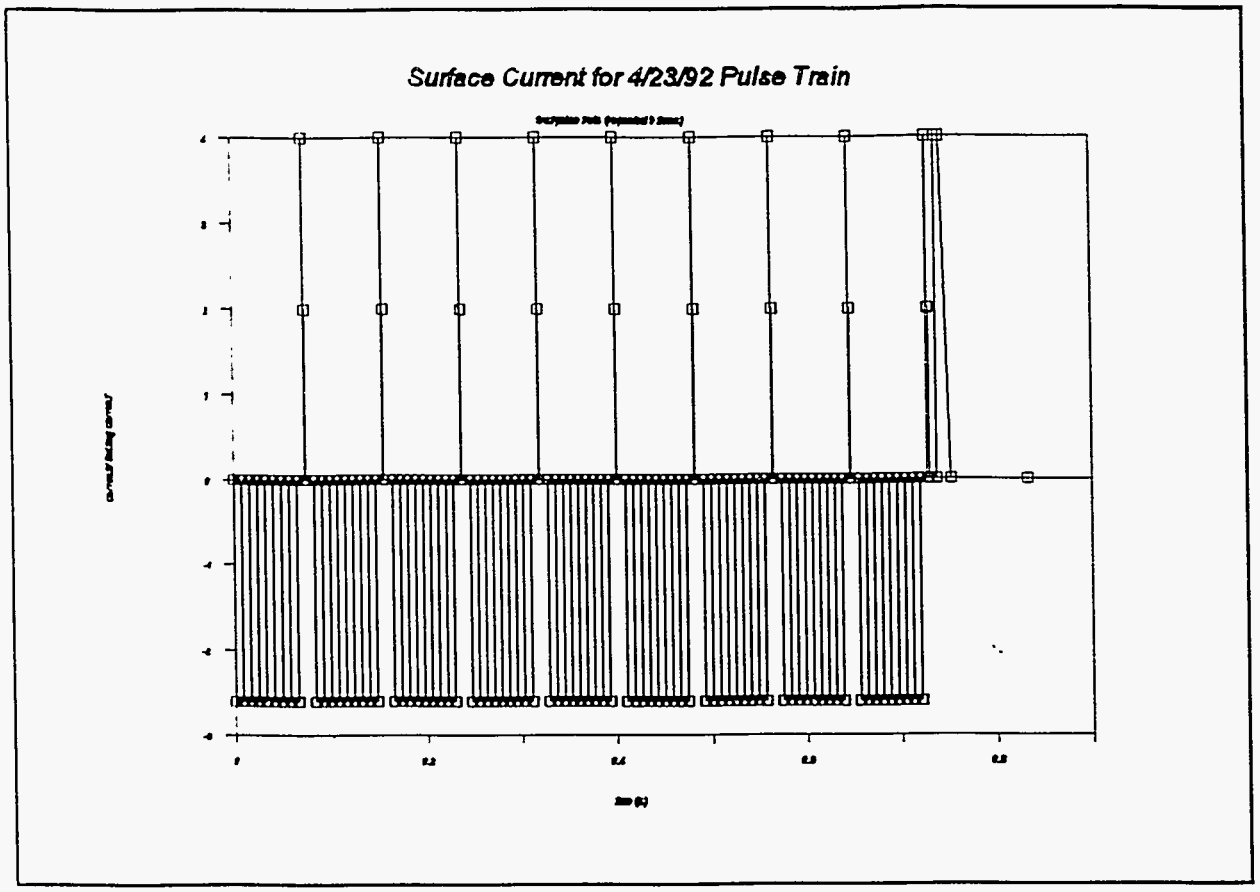

Figure 2. Plot of surface current for first two levels of a multilevel fractal waveform. Cathodic (plating) pulses are below zero; anodic (deplating) pulses are above zero.

The F_{net} as defined was typically 0.40 for the overall waveform. This value was obtained for a 4-level fractal by deplating at each level 20% of the material deposited at that level. The fraction remaining then becomes $(0.8)^x = (0.8)^4 = 0.4$. To achieve the same F_{net} with fewer levels, the fraction removed at each level is adjusted. For comparison, the F_{net} was held constant for many of the experiments, while adjusting the number of levels, relative cathodic and anodic pulse amplitudes, anodic pulse shape and duration, and repeat values and cathodic duty cycle values.

The fractal structure described can be considered a framework for generating anodic pulse duration choices of widely varying values. In the language of experimental design, this can be called an aggressive design strategy, which covers a large design space (2X to 2000X the cathodic pulse duration, for example). It is not necessary to use each of the levels defined by simple application of the fractal model. For example, one could use durations of 2X and 200X, but not 20X and 2000X, to generate a 2-level design. If the presence or absence of an anodic pulse with a given pulse duration can be represented by the binary 0 or 1, then if 4 possible levels exist for a given design and each level can be either present or not present, there are 16 possibilities as shown in Figure 3. These possibilities range from no anodic pulses at [0000], to a simple periodic-reverse at [1000], to a full 4-level fractal at [1111]. The 2-level fractal mentioned earlier would have the binary representation [1010]. This type of representation can be one of the variables used to create experimental designs for fractal waveform experiments. Later in this paper, comparison of experimental results against this representation is shown.

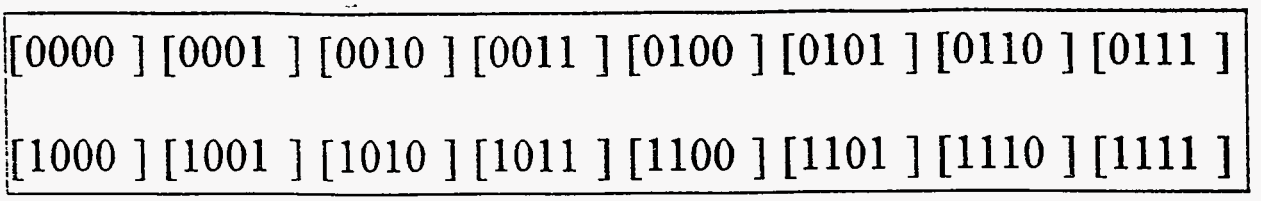

Figure 3 -Binary representation of the possible distributions of anodic current within the structure of a 4-level fractal waveform

Diffusion Considerations

As for any plating situation, there are current density limitations to the process that are affected by both the concentration and diffusion coefficient of the depositing species and the mass transfer conditions. For this study, we used a lead-plating bath which is essentially the same as described by Wiesner[2]. A plating system similar to this bath was studied extensively by Roha[3]. The relevant concentrations and diffusion coefficients for this system were used to explore possible diffusion limitations to parameter values used in this work. Rather than use only the time-averaged current density to calculate a gross situation, the actual fractal structure (such as in Figure 2) was used as input to a thermal/mass transport code. The diffusion calculations were done using HEATING[4], a finite difference code intended for heat transfer calculations. It is written in FORTRAN and can be run on platforms as small as a 386 PC[5]. Although HEATING is intended for thermal diffusion, a straightforward transformation of variables allows it to be used for mass diffusion.

The diffusion calculations were done in one dimension. Boundary conditions were defined at the outer edge of the diffusion layer and at the surface of the part. The concentration at the outer edge of the diffusion layer was set to the value in the bulk liquid. In the transformed units, the bulk value is 1300 (this is somewhat arbitrary). At the solid surface, a time-dependent flux was applied that corresponded to the current specified for the plating/deplating pulse pattern. The initial condition was that the lead ion concentration was equal to the bulk concentration throughout the calculational domain. The enclosed plots show results for two different cases. Both cases used cathodic pulses of amplitude 1.3 A cm^{-2} and anodic pulses of amplitude 2.0 A cm^{-2}. For one case (Figure 4), the diffusion layer was 0.012 cm thick and represented a boundary layer thickness calculated for a particular rotating part. This case simulated a part that was rotating in the tank rapidly enough so that the solution could be considered well stirred; thus, the ion concentration at the outer edge of the diffusion layer was constant. For the other case (Figure 5), the diffusion layer was thick enough so that the effect of the surface flux was not detectable at the diffusion boundary. This simulated a very large tank of stagnant solution. Note that the thickness of the diffusion layer is the momentum boundary-layer thickness multiplied by a function of the Schmidt number.

The plots show the concentration of the lead ion at the surface. For the case with infinite boundary layer thickness, the ion concentration becomes negative during some portions of the waveform. That is not physically plausible. Rather, the result shows that, for the assumed diffusion constant, bulk ion concentration, and pulse amplitude, diffusion from an infinite reservoir at an infinite distance *is not* a strong enough mechanism to provide the needed amounts of ions. For the case with a 0.012-cm boundary-layer thickness, the surface concentration remains positive.

The result indicates that diffusion from a well-stirred reservoir across a boundary layer of that thickness *is* a strong enough mechanism to provide the needed amounts of ions. Note that while the analysis was done to show the effect of mass transfer changes, changing the balance of cathodic to anodic current pulse amplitude would also lead to mass transfer problems which can likewise be modeled by simply changing the values input to HEATING.

The general problem of understanding the mass transfer characteristics during electroforming is very important to controlling the process. For objects that are very complex, with little symmetry, only a full numerical analysis will be useful. However, for rotating axisymmetric mandrels, Kirkpatrick has developed treatments[6] that can estimate diffusion boundary layer thicknesses as a function of position on the mandrel, which can be used in numerical or analytical

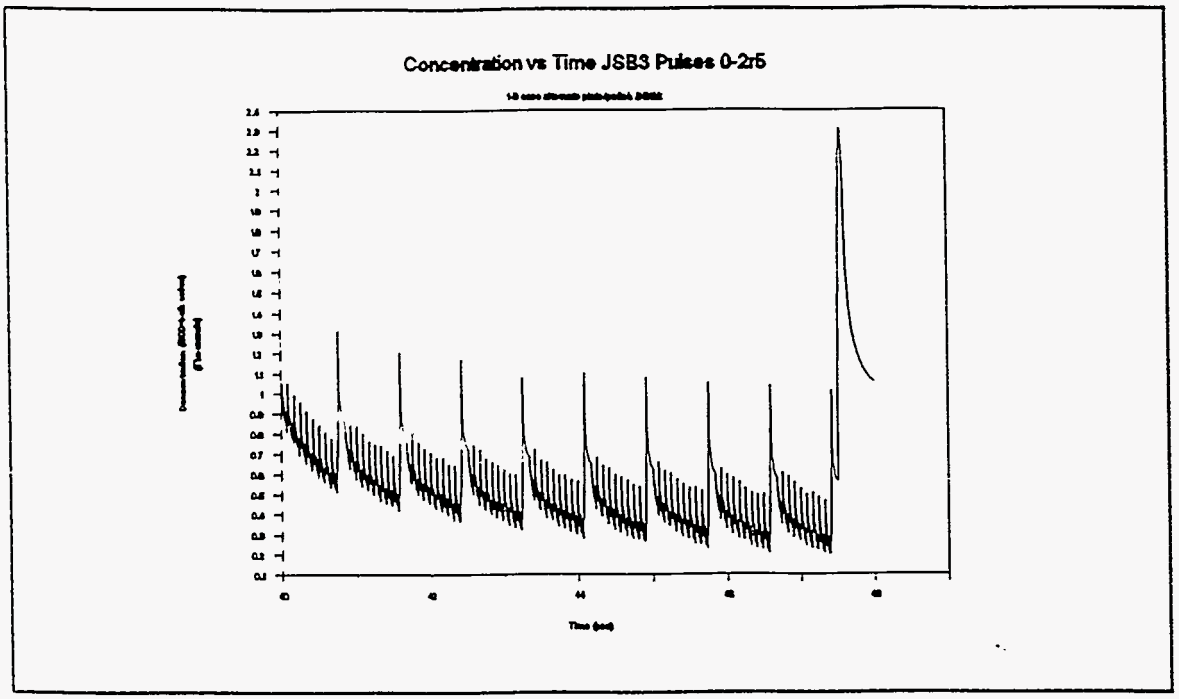

Figure 4 Plot of surface concentration for restart 5 (6th cycle of pulses). Case uses diffusion layer thickness 0 012 cm (well-stirred).

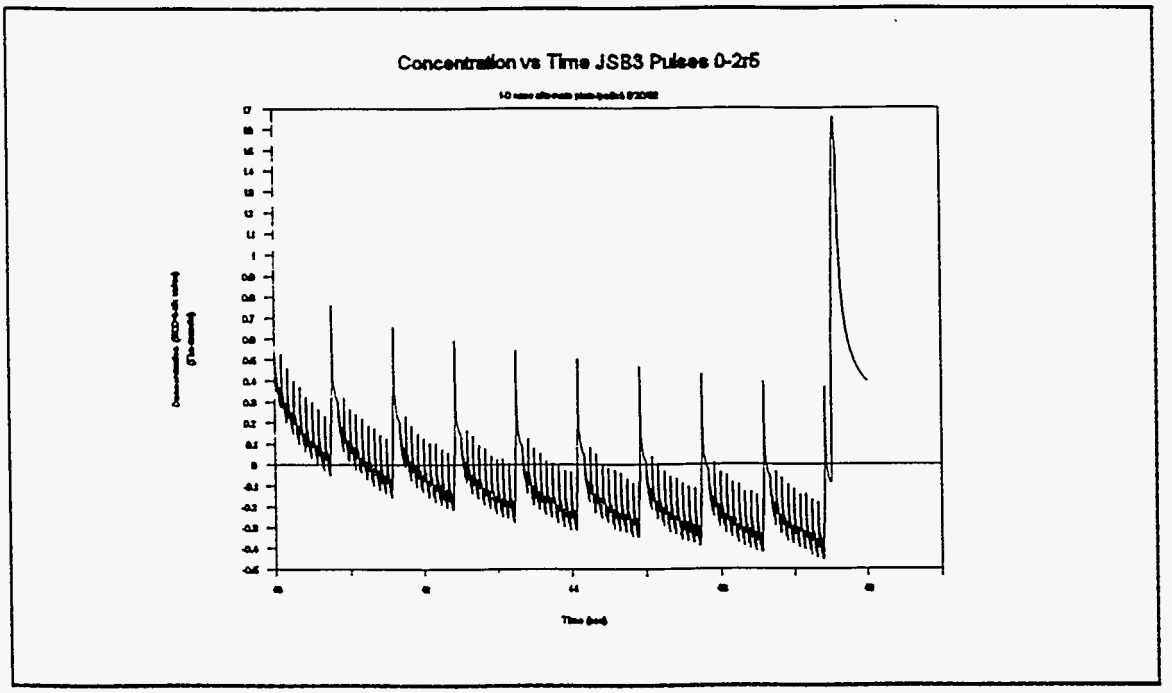

Figure 5. Plot of surface concentration for restart 5 (6th cycle of pulses). Case uses "large" boundary-layer thickness (stagnant).

calculations of current density distribution. Numerical calculations can be based on finite difference, finite element, or boundary element methods.

Experimental

Apparatus and Hardware

Figure 6 illustrates the physical setup and plating waveform generation system. The plating cell used a stainless steel mandrel and a lead-sheet consumable anode. The mandrel was a hemisphere of radius 0.5 cm, protruding from a polytetrafluoroethylene (PTFE) cylinder, and was rotated by a stepper motor under the

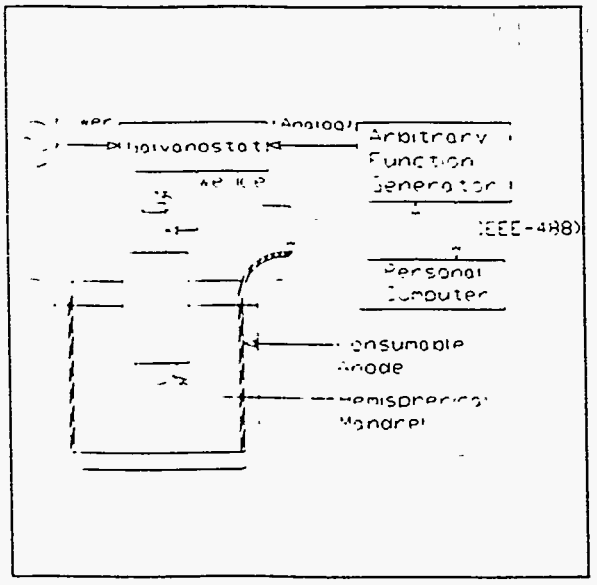

Figure 6 - Description of the system used in electroforming tests using fractal waveforms and the lead fluoborate bath with consumable lead anode.

control of the system computer through an RS-232 port. Rotation speed was typically 200 rpm; however, it was possible to vary this speed during the experiment. For certain experiments with multisecond longest-anodic pulses, rotation was stopped to achieve stagnant conditions mimicking electropolishing.

The mandrel shaft was insulated from the stepper motor, and current was bussed to the rotating shaft through two opposed carbon brushes. The surface of the mandrel was a machined surface of finish about 40μin rms, except for certain cases where a mandrel polished using 0.05 μm diamond abrasive was used. The device supplying the controlled-current waveform to the plating cell was a 10-A potentistat/galvanostat, with 20-V compliance voltage, operated in the galvanostatic mode. This essentially acts as a programmable controlled-current power supply.

In turn, the galvanostat was programmed using an analog signal from an arbitrary-function generator. The generator used for these experiments had an 8K memory; i.e., up to 8192 discrete steps could be used to define the waveform, which was adequate to store 4-level fractal waveforms, although they were a tight fit. Other similar generators are now available that have 32K or even 64K memories, which would simplify waveform storage, increase available resolution, and permit more than one waveform to be kept in memory at one time. The clock speed of the generator sets the time per step; for most of these designs, it was set to 1 ms, equal to the length of time for the plating pulse. Alternate clock speeds were programmed to apply the initial DC strike, which was 32 mA cm^{-2} for 5 min. As soon as the strike was completed, the generator began to apply the fractal waveform, repeating the waveform as many times as desired for the particular experiment.

In turn, the generator was given instructions, through the IEEE-488 interface, from a personal computer. A program was created for the PC that generated a string of commands and values that when downloaded to the generator would store the desired waveforms in memory. Initially, this program relied on manual operations of duplication and copying to create the command and value string, in the manner of a primitive spreadsheet. A later version permitted the input of a limited set of fractal parameters, allowing the program to apply recursive operations to generate the complete command and value string.

The plating bath (after Weisner) was about 0.5 M in lead fluoborate, with additions of boric acid, coumarin and sodium lignosulfonate. This bath is designed for DC operation, but no prior experience of its use in pulsed plating was known.

Experimental Procedure

Waveforms of the design required were generated on the PC: separate waveforms were created for the initial strike, the main waveform, and any multisecond anodic sections. These waveform files were referenced in an experiment file, which instructed the computer to download them to the arbitrary function generator and to tell the generator which waveforms to use and in what order.

The mandrel (either the machined or the polished one) was cleaned with detergent and water and alcohol rinsed, then installed in the PTFE insulator. Packing and a PTFE washer were used inside the insulator to seal against solution infiltration and to keep the mandrel shaft centered. The mandrel shaft was assembled with a dust shield, a carbon-brush block, an insulator and a stepper motor, and secured with the mandrel centered in the plating cell.

A portion of lead-plating bath was added to the cell to immerse the mandrel about 3 to 4 cm below the surface. All experiments were performed at room temperature, which was a relatively steady 25 °C. The computer was instructed to begin the experiment, and an initial strike under rotation was applied, after which plating was continued for typically 5 to 6 hours

When plating was terminated, the mandrel was disassembled from the system, rinsed clean, and dried. Photographic records were made using a camera accessory for a stereo microscope. Because the plate typically extended past the hemisphere equator onto the plane adjacent to the insulator body, this part of the plate was trimmed off with a sharp knife (the mandrel surface had not been prepared such as to cause metallurgical bonding of the plate) and saved. The body of the electroformed hemishell was separated from the mandrel using thermal shock; three cycles of dipping into liquid nitrogen followed by dipping into water were used, which almost invariably allowed pulling the electroform free with minimal force. The hemishell and the trimmings were cleaned, dried and weighed to a precision of 10 μg. The deposit was then submitted for testing such as scanning electron microscopy (SEM), sectioning for microstructural analysis, or other methods as appropriate.

Surface Morphologies and Microstructures Obtained

Figures 7 through 20 show various electroform morphologies (and in some cases, associated microstructures) obtained using a variety of waveform designs. Table 1 summarizes morphology results for all binary representations and cathodic pulse amplitudes tested.

Figure 7 shows for comparison a plate made using DC at -0.0396 A cm^{-2}. Quite level, it is, however, not shiny and is nodular on a micro scale. Figures 8 and 9 show results of designs with only plating pulses, with P_c values of -0.96 A cm^{-2} and equivalent CD of -0.0282 A cm^{-2} in one case, and -1.05 and -0.0396 in the other. Increasing the pulse amplitude and mean CD changes a low nodular structure to one with extended nodules and dendrites.

Figure 10a, 10b and 10c shows macro, micro cross section, and surface SEM views, respectively, of a case with intermittent deplating pulses [0001], P_c = -1.05 A cm^{-2}, the anodic pulses having an amplitude of 1.28 A cm^{-2} and a trapezoidal shape. The macro view shows that both rings and spirals are produced under these conditions. The 400X micro section was taken at the edge next to the mandrel, and shows the strike and the transition to a banded structure with a number of bands equal to the number of repetitions of the waveform (170). The 2000X SEM surface view shows that, for this case, where all the deplating current is put into long pulses at long intervals, a porous surface is obtained that also has octahedrally-shaped adherent particles.

Figure 11a and 11b shows the macro view and a 2000X SEM view, respectively, of a case with P_c = -1.05 A cm^{-2} and periodic deplating pulses [1000] of 1.28 A cm^{-2}, with equivalent CD of -0.0334 A cm^{-2}. The SEM view reveals a reasonable quality plate over most of the surface, but the macro view shows the presence of "hydra"-shaped dendrites (dendrites extending from the end of nodules). When anodic pulse amplitude is boosted to 2.26 A cm^{-2} as in Figure 12, this irregularity disappears, and a smooth, good-looking plate results.

When the pulse structure is changed to [1100], as for Figure 13, with P_C = -1 05 A cm^{-2}, anodic pulses of 1 28 A cm^{-2} and equivalent CD = -0.0351 A cm^{-2}, hydra dendrites are obtained. Figure 14a and 14b shows what happens when the pulse structure is changed to [1010] with the same pulse amplitudes (but CD = -0.0411 A cm^{-2}). Only low nodules are seen, but the surface has an etched texture and a small number of octahedral particles adhere to the surface.

Changing the pulse structure further to [1110] gives the results shown in Figures 15a, 15b and 16. Figure 15a and 15b shows the result of using P_C = -1 05 A cm^{-2} and anodic pulse amplitudes of 1.05 A cm^{-2}, with equivalent CD = -0 0402 A cm^{-2}. Figure 15a gives the macro view, and 15b gives an SEM image at 300X. Many platelets and small octadedra are observed. The conditions for the sample of Figure 16 change in that anodic pulse amplitudes of 1.28 A cm^{-2} are used and an equivalent CD = -0 0394 A cm^{-2} results. This surface is smoother than that of Figure 14, but low nodules are prolific.

Specimens created with the full 4-level [1111] fractal are shown in Figures 17 through 19 for a consistent P_C = -1 05 A cm^{-2}, but a varying anodic pulse amplitude (and shape). For Figure 17, triangular anodic pulses of amplitude 0.96 A cm^{-2} were used, and an equivalent CD of -0 0354 A cm^{-2} resulted. For Figure 18, the anodic pulses were changed to 1.28 A cm^{-2} with a rectangular shape and an equivalent CD of -0.0284 A cm^{-2}. For figure 19, this changes to 1 92 A cm^{-2} and CD = -0 0264 A cm^{-2}. The smoothness of the surface improves through this progression. The F_{net} changes through this progression from 0.4085 to 0.3223 to 0.3006.

Figure 20a-f focuses on the same conditions as those for the specimen of Figure 18, except that trapezoidal anodic pulses are used. Figures 20a and 20b show the surface macro and the cross-section views, respectively, of the plated body. Figures 20c and 20d show the polished and etched microstructure, respectively, with preparation and lighting conditions changed for 20d so that the fine layered structure can be seen. Approximately the same number of layers appear in the micrograph as the number of repetitions of the waveform during the plating operation. Figure 20e and 20f shows the SEM view of the outer surface at 400X and 2000X, respectively, revealing an interesting etched pattern.

All of the preceding figures are of specimens produced using machined mandrels, but certain runs in this experimental program were done with polished mandrels. The presence of "rings" on the specimens was always associated with machined mandrels and their inevitable machining grooves; when polished mandrels were used, no rings were observed. Indeed, when the conditions of Figure 19 were duplicated using a polished mandrel, the results were very similar, except that very little splotchiness was seen.

Use of Fractal Waveforms as Analytical Probes

To obtain information about the status of electrodes and the characteristics of electrode reactions, one common practice is to measure electrode impedance *vs* the frequency of a signal applied to the electrode. Such information is measured from the millihertz to the megahertz range. To obtain this information for the low-frequency part of the spectrum (lower than 10 Hz), common practice is to create a signal which is a composite of about 20 low-frequency signals, apply this composite to the electrode, and analyze the response using a mathematical transformation such as the fast Fourier transform (FFT). Both sinusoidal and square-wave composite signals have been used for this purpose. Figure 21 shows such a composite signal waveform using square waves.

Fractal waveforms such as that shown in Figure 22 are basically different from these composite waveforms in that they are not composed of combinations of sinusoids or other periodic forms that are symmetrical about an axis. However, they do have periodicity and significant, complex information content, and thus may be useful as probes of electrode reactions. How to approach the analysis of fractal waveform signals is an open question. The FFT has been described in many places and will not be repeated here, but the results of applying the FFT to both the square wave composite and the fractal waveform example are shown in Figures 23 and 24. Because of a difference in overall amplitude of the two waveforms, a comparable difference exists in the magnitude value results from the two cases. A comparison of the magnitude components shows a considerable amount of energy across the spectrum for both waveforms, although the low-frequency end for the square-wave composite seems richer.

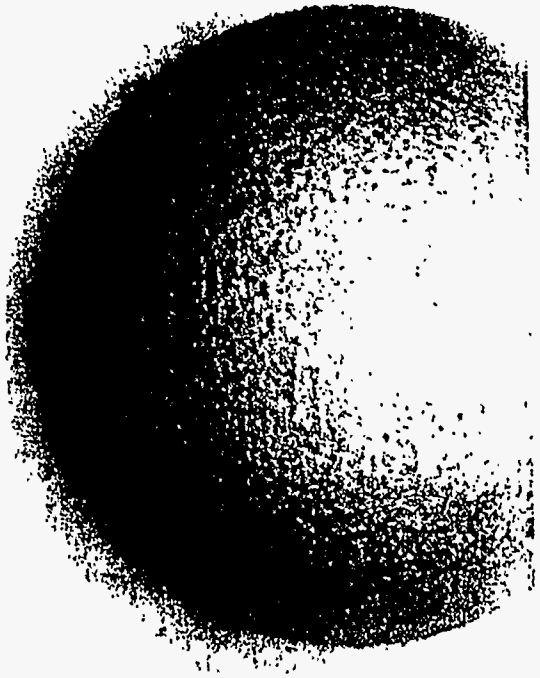

Figure 7 - Macro View of Lead Electroform Made Using DC @ - 0.0396 A cm^{-2} (Code 093091)

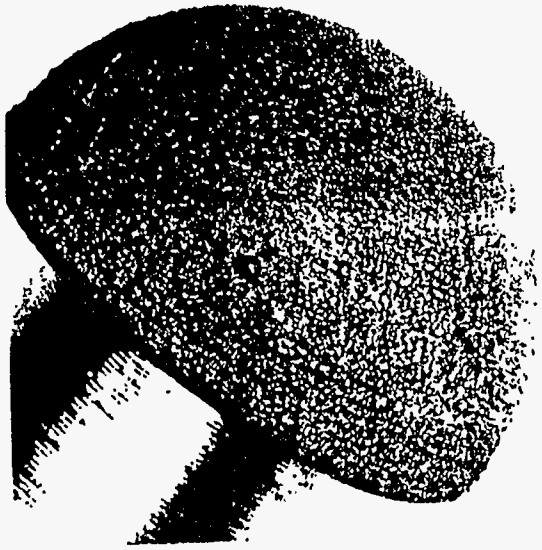

Figure 8 - Macro View of Lead Electroform Made Using Pulsed Current Design [0000] with P_c = - 0.96, CD = - 0.0282 A cm^{-2} (Code 081491)

Figure 9 - Macro View of Lead Electroform Made Using Pulsed Current Design [0000] with P_c = - 1.05, CD = - 0.0396 A cm^{-2} (Code 092791)

Figure 10a - Macro View of Lead Electroform Made Using Pulsed Current Design [0001] with P_C = - 1.05, P_A = 1.28, and CD = - 0.0404 A cm^{-2} (Code 010992)

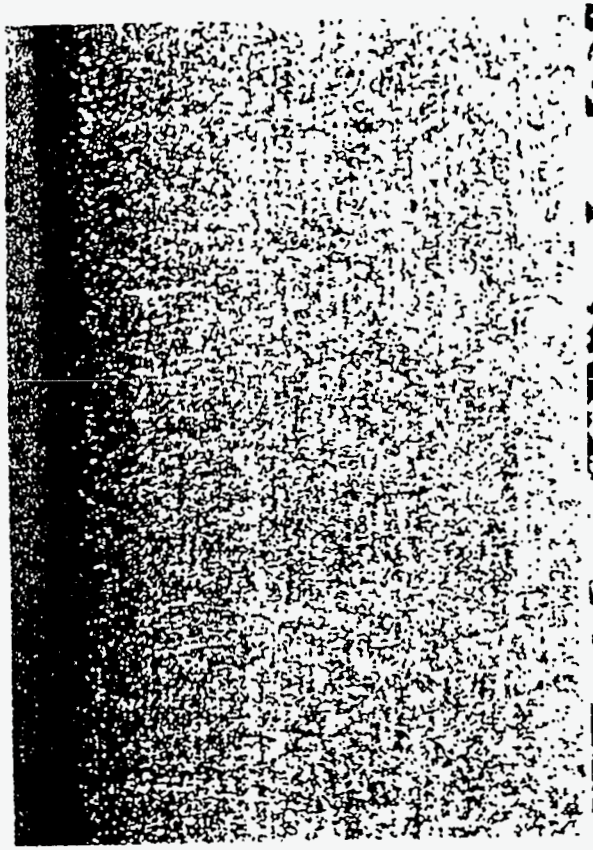

Figure 10b - Micro View (400X BF) of Cross-Section of Lead Electroform of Fig. 10a

Figure 10c - SEM View (2000X) of Surface of Lead Electroform of Fig. 10a

Figure 11a - Macro View of Lead Electroform Made Using Pulsed Current Design [1000] with P_C = - 1.05, P_A = 1.28, and CD = - 0.0334 A cm^{-2} (Code 122091)

Figure 11b - SEM View (2000X) of Surface of Lead Electroform of Fig. 11a

Figure 12 - Macro View of Lead Electroform Made Using Pulsed Current Design [1000] with P_C = - 1.05, P_A = 2.26, and CD = - 0.0395 A cm^{-2} (Code 092591)

Figure 13 - Macro View of Lead Electroform Made Using Pulsed Current Design [1100] with P_C = - 1.05, P_A = 1.28, and CD = - 0.0351 A cm^{-2} (Code 030592)

Figure 14a - Macro View of Lead Electroform Made Using Pulsed Current Design [1010] with P_C = - 1.05, P_A = 1.28, and CD = - 0.0411 A cm^{-2} (Code 031892)

Figure 14b - SEM View (1000X) of Surface of Lead Electroform of Fig. 14a

Figure 15a - Macro View of Lead Electroform Made Using Pulsed Current Design [1110] with P_C = - 1.05, P_A = 1.05, and CD = - 0.0402 A cm^{-2} (Code 051892)

Figure 15b - SEM View (300X) of Surface of Lead Electroform of Fig. 15a

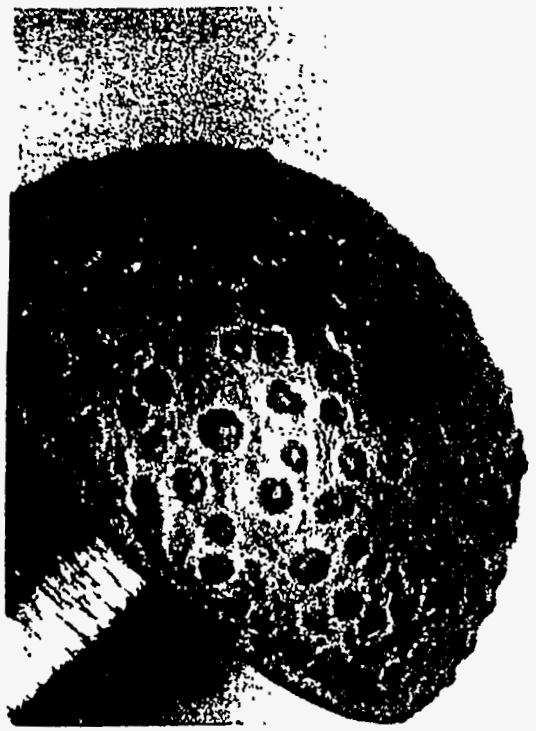

Figure 16 - Macro View of Lead Electroform Made Using Pulsed Current Design [1110] with P_C = - 1.05, P_A = 1.28, and CD = - 0.0394 A cm^{-2} (Code 030992)

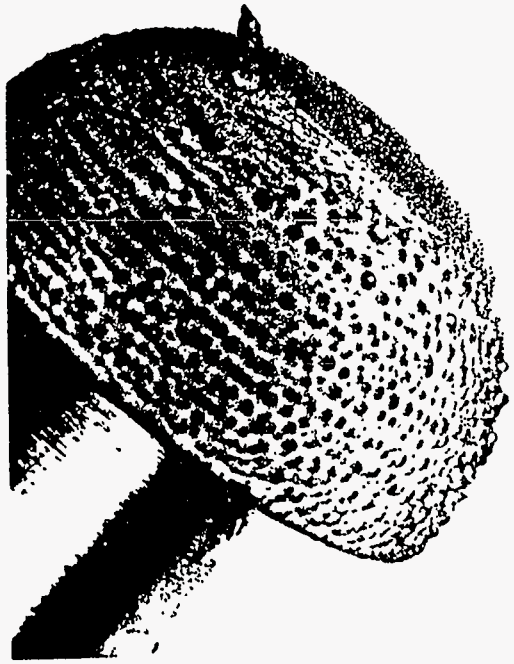

Figure 17 - Macro View of Lead Electroform Made Using Pulsed Current Design [1111] with P_C = - 1.05, P_A = 0.96, and CD = - 0.0364 A cm^{-2} (Code 100491)

Figure 18 - Macro View of Lead Electroform Made Using Pulsed Current Design [1111] with P_C = - 1.05, P_A = 1.28, and CD = - 0.0284 A cm^{-2} (Code 121691)

Figure 19 - Macro View of Lead Electroform Made Using Pulsed Current Design [1111] with P_C = - 1.05, P_A = 1.92, and CD = - 0.0264 A cm^{-2} (Code 121391)

Figure 20a - Macro View of Lead Electroform Made Using Pulsed Current Design [1111] with P_C = - 1.05, P_A = 1.28, and CD = - 0.0324 A cm^{-2} (Code 121891)

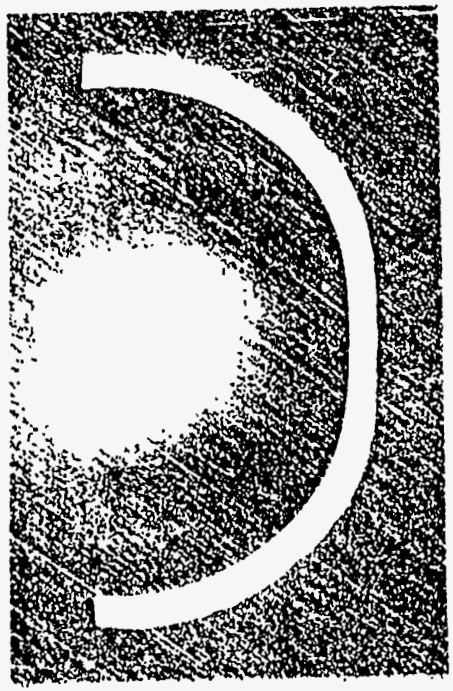

Figure 20b - Macro View (7X BF) of Cross-Section of Lead Electroform of Fig. 20a

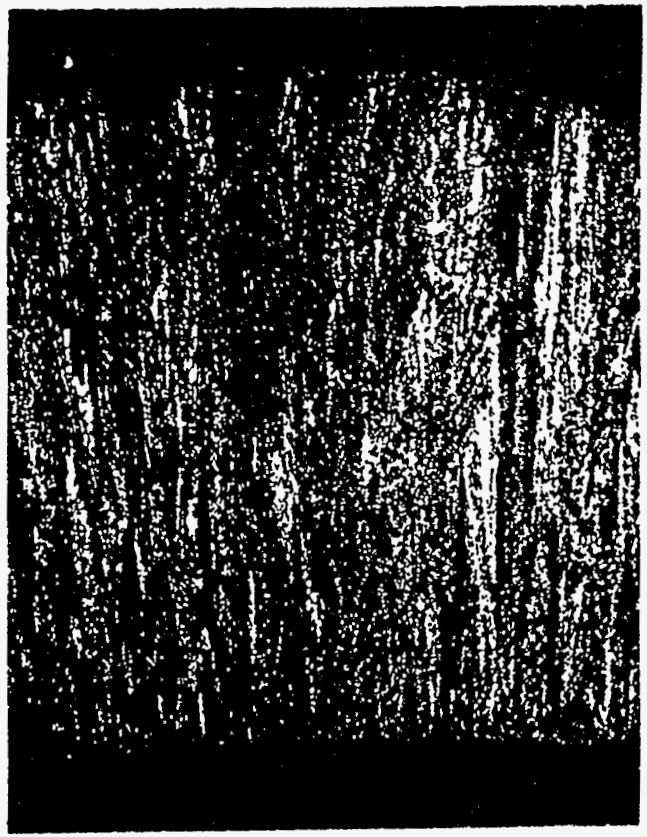

Figure 20c - Micro View (150X PL) of Cross-Section of Lead Electroform of Fig. 20a

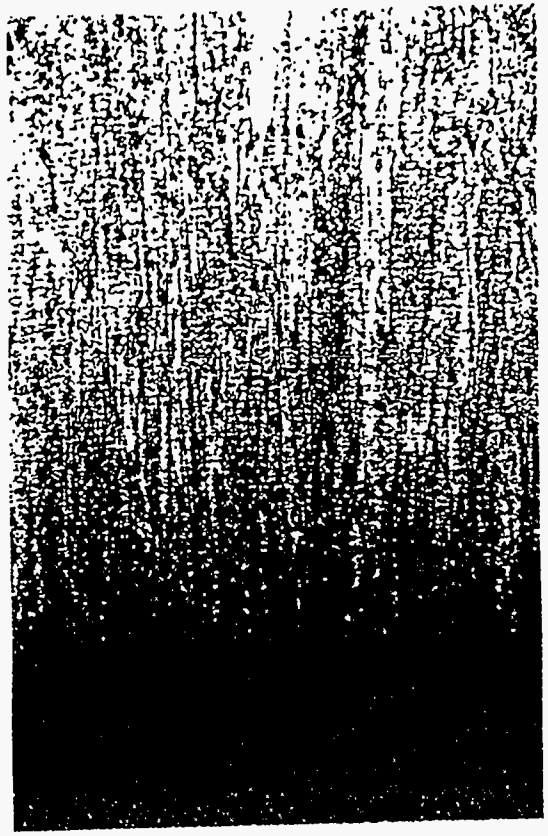

Figure 20d - Micro View (400X oblBF) of Cross-Section of Lead Electroform of Fig. 20a

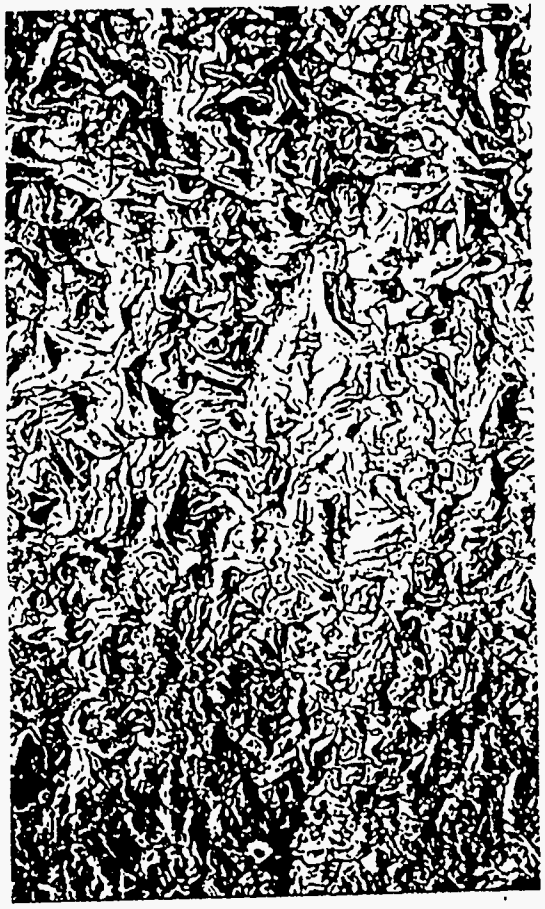

Figure 20e - SEM View (400X) of Surface of Lead Electroform of Fig. 20a

Figure 20f - SEM View (2000X) of Surface of Lead Electroform of Fig. 20a

Table 1 - Comparison of Surface Morphologies against Binary Representation and Cathodic Current Density

Waveform Binary Representation	For P_C = 0.90 or 0.96 A cm^{-2}	For P_C = 1.02 or 1.05 A cm^{-2}	For P_C = 1.20 A cm^{-2}
DC	Very smooth @-0.044 A cm^{-2}	————	Level @- 0.062 A cm^{-2}
[0000]	~ 280 small nodules	~ 280 long nodules, dendrite	----------
[0001]	Smooth, no rings, fine spirals	Smooth, both rings and spirals; sponge-like surface	----------
[0010]	----------	----------	----------
[0011]	----------	----------	----------
[0100]	----------	----------	----------
[0101]	----------	----------	----------
[0110]	----------	----------	----------
[0111]	----------	----------	----------
[1000]	Small nodules; no rings or spirals or dendrites	Smooth for P_A = 2.26 A cm^{-2}; w/ 28 hydra dendrites for P_A = 1.28 A cm^{-2}	----------
[1001]	----------	----------	----------
[1010]	----------	Spirals; ~ 180 low nodules; no rings	----------
[1011]	----------	----------	----------
[1100]	----------	No spirals or rings, but ~ 80 hydra dendrites for P_A = 1.28 A cm^{-2}	----------
[1101]	----------	----------	----------
[1110]	----------	Faint spirals, ~ 180 low nodules for P_A = 1.28 A cm^{-2}; rings w/ many small nodules for P_A = 1.05 A cm^{-2}	----------
[1111]	Rings, few small nodules, no spirals, no dendrites; to very smooth w/ rings dep. on P_A*	Rings, moderate nodules, slight spirals; to very smooth but splotchy appearance dependent. on P_A*; microetched surface	Rings, many small nodules, no spirals*

* NOTE: for polished mandrels, no rings, but spirals become obvious.

It may be that, because of the nature of the fractal waveform, transformations other than the FFT are more appropriate. One strictly digital transformation is the Walsh Transform[8]. A precedent exists for using Walsh functions and transforms to analyze electrolytic systems. A recent paper[9] describes the use of "random" pulses applied to a corroding system in a Walsh-function pattern, the resulting voltammetric data being analyzed by a Walsh transform to reveal patterns indicative of various corrosion states. Figures 25 and 26 show the result of applying the Walsh transform to the composite square wave and the fractal waveform, respectively. This transform returns only a magnitude vs a parameter called "sequency", which is an analog to frequency. The two patterns are rich in low-sequency content, but the fractal case shows a grouping that might relate to the fractal levels.

At this point, there is no clear indication of how this analysis might be used; however, it appears that some such method might be identified to take advantage of the properties of the fractal waveform for analytical purposes.

Current Efficiency

The current efficiency (CE) for deposition is defined as the number of coulombs equivalent to the weighed amount of material deposited (assuming the entire deposit to be 100% lead and the valence of lead to be 2) divided by the net number of cathodic coulombs ($C_c - C_a$) applied to the plating cell (as determined numerically from the waveform definition). If one assumes simple, 100% efficient electrode reactions, this number should have been 1.000 in each case. The value obtained actually varied from 0.795 to 1.339 with a mean of 0.978. Apparent differences existed between experiments using different anodic pulse shapes (triangular *vs* rectangular *vs* trapeziodal); however, that variable is confounded with time in the overall experimental program, so no clear relationship can be verified.

Discussion

Possible causes of variation in CE may include the following: numerical errors in determining the actual number of net cathodic coulombs passed; cathodic side reactions, including reduction of additives and discharge of hydrogen ion; anodic side reactions, including evolution of oxygen gas and conversion of lead to PbO_2 or other species ; and drift in equipment calibration. Because of the discovery of octahedral and platelet-shaped phases on the deposit surface, the existence of anodic side reactions seems likely. It should be noted that this is a problem which is particularly significant for lead. (Actually, the observations reported here may have some relevance to the use of pulsed chargers/reconditioners for lead storage batteries.) All of the non-experimental-error possibilities might be affected by the pulse shapes used.

The choice of plating bath for this study was influenced by having the lead bath available as a well characterized system (albeit for DC plating), as well as the known high exchange current for lead deposition. High exchange currents are generally associated with tendancies to generate dendrites and other morphological instabilities. Thus, the lead bath is a sensitive test vehicle for methods to control plating irregularities. However, the presence of additives, especially of lignosulfonate, which has a very large molecular weight and thus likely diffuses significantly slower than lead, probably tends to confuse interpretation of results. Thus, an argument would seem to exist for using simpler baths with minimal additives, to determine more clearly the effects of waveform design choices.

The use of the binary representation [XXXX] as a parameter for experimental design for fractal waveforms seems warranted. One could relate the value of this binary number to the complexity of the waveform. Another controlling factor might be the length of time used in the longest anodic pulse, with waveform complexity as a modifying factor. Other variables would be cathodic pulse amplitude and pulse width, cathodic pulse duty cycle, anodic pulse amplitude and pulse width, off-time before and after applying the anodic pulse, and the overall F_{net} and its value for each level.

Clearly, polished mandrels provide a better initial surface on which to begin plating. No nuclei exist to encourage the growth of irregularities. Even if conditions of plating were such as to encourage nodular growth, these nodules were finer and more uniform when polished mandrels were used. Use of polished mandrels might change the nodular pattern, from rings and no spirals, to spirals and no rings. Machining grooves on a rotating mandrel can possibly change slightly the hydrodynamic conditions and interfere with the development of resonant structures such as those

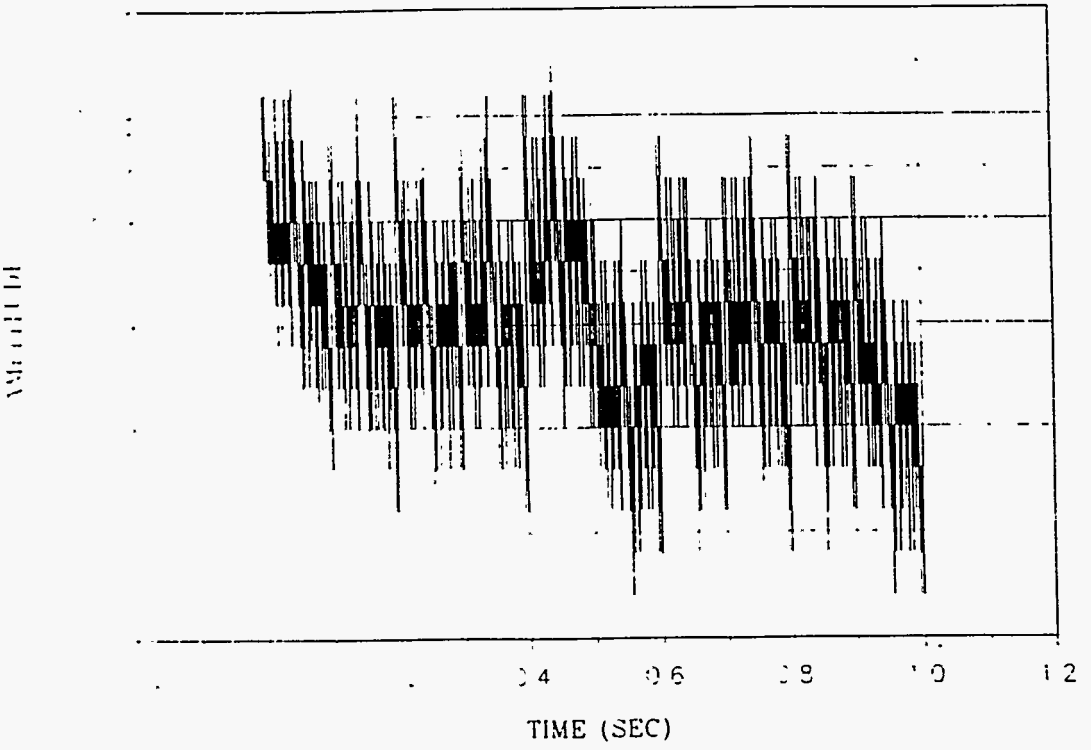

Figure 21 - Waveform Composed of a Composite of Square Waves (16384 points) as Input to Analysis

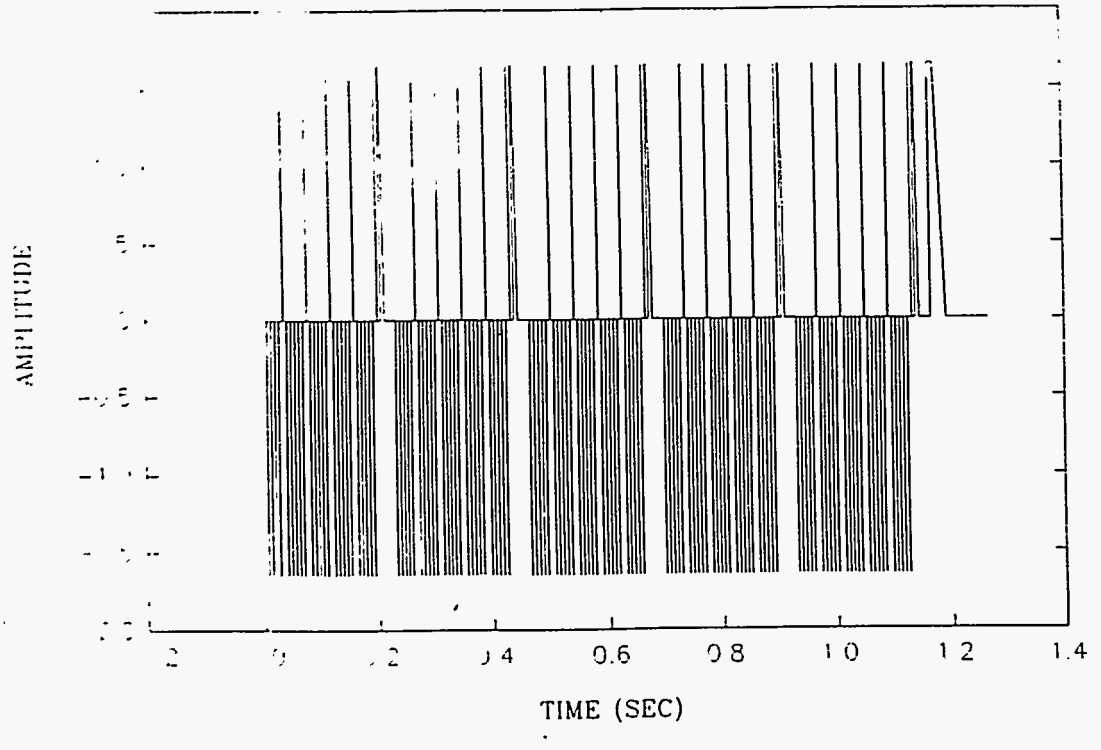

Figure 22 - Fractal Waveform Used as Input to Analysis

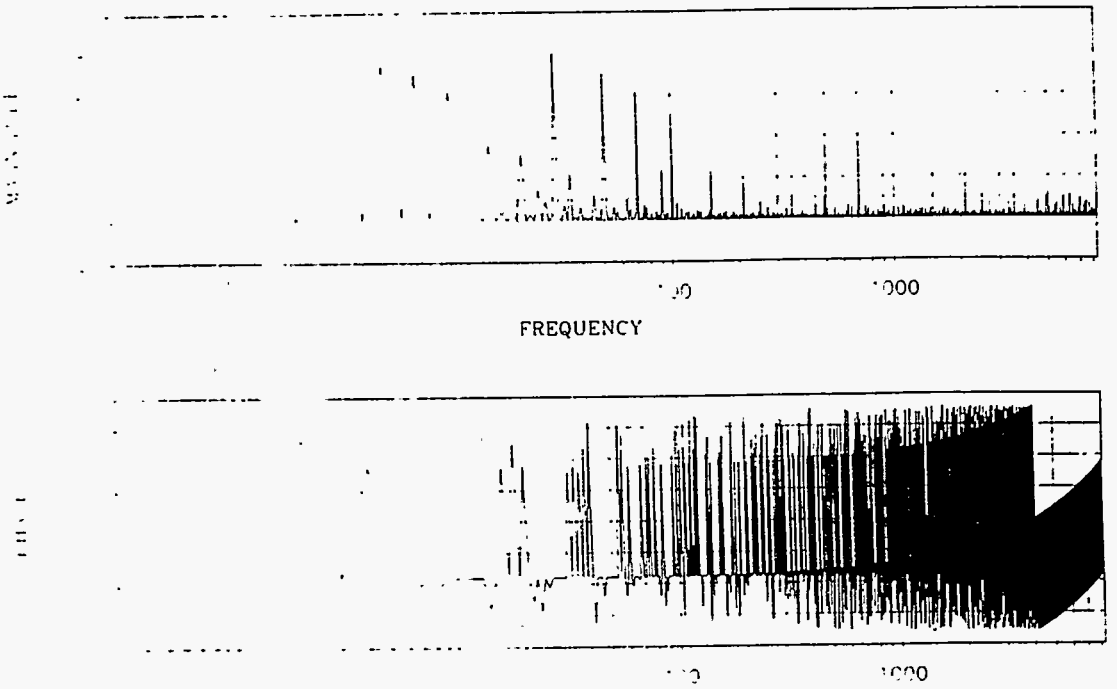

Figure 23 - Result of FFT Analysis of Square Wave Composite

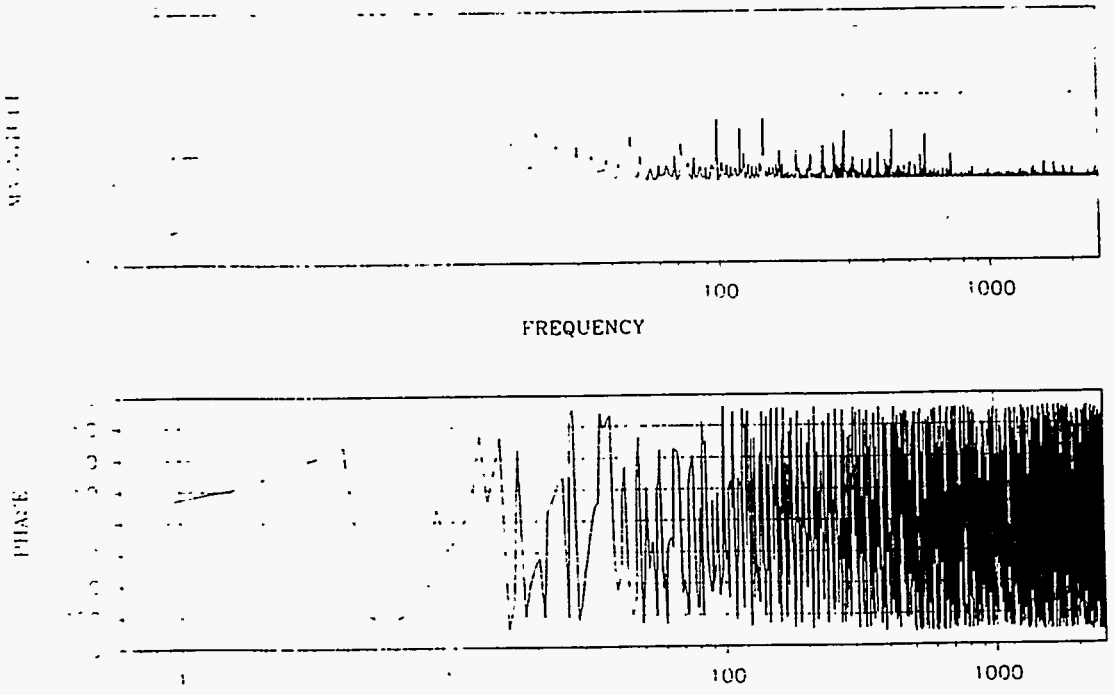

Figure 24 - Result of FFT Analysis of Fractal Waveform

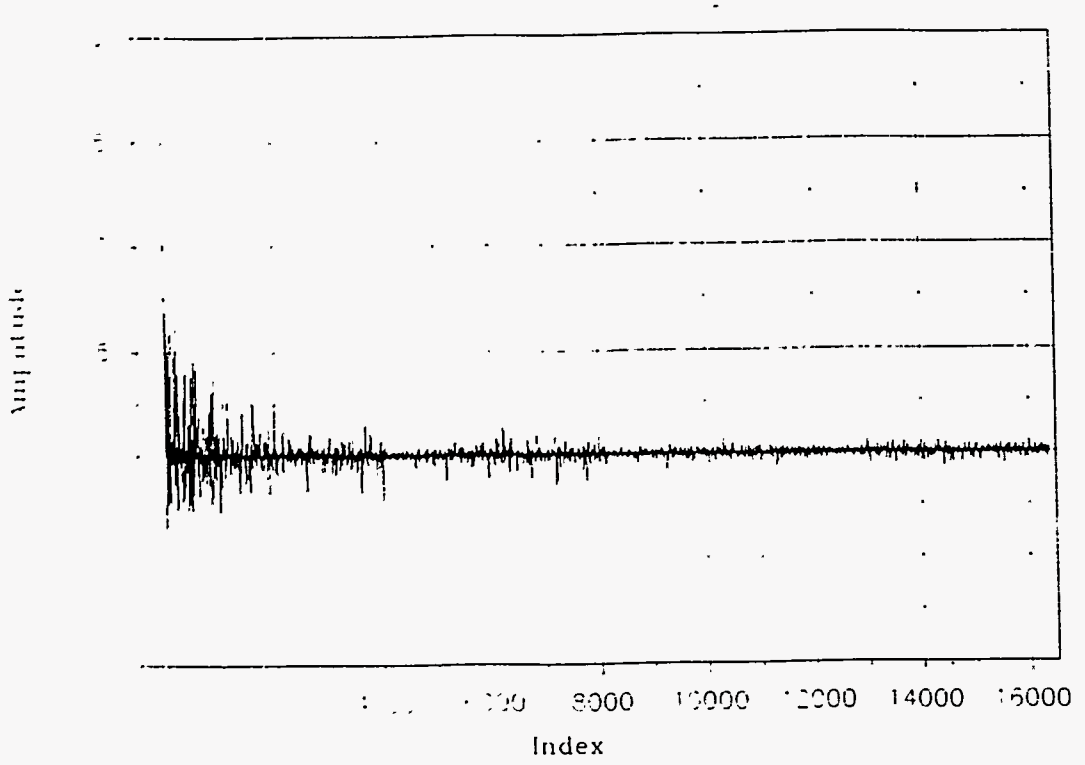

Figure 25 - Result of Walsh Transform Analysis of Square Wave Composite

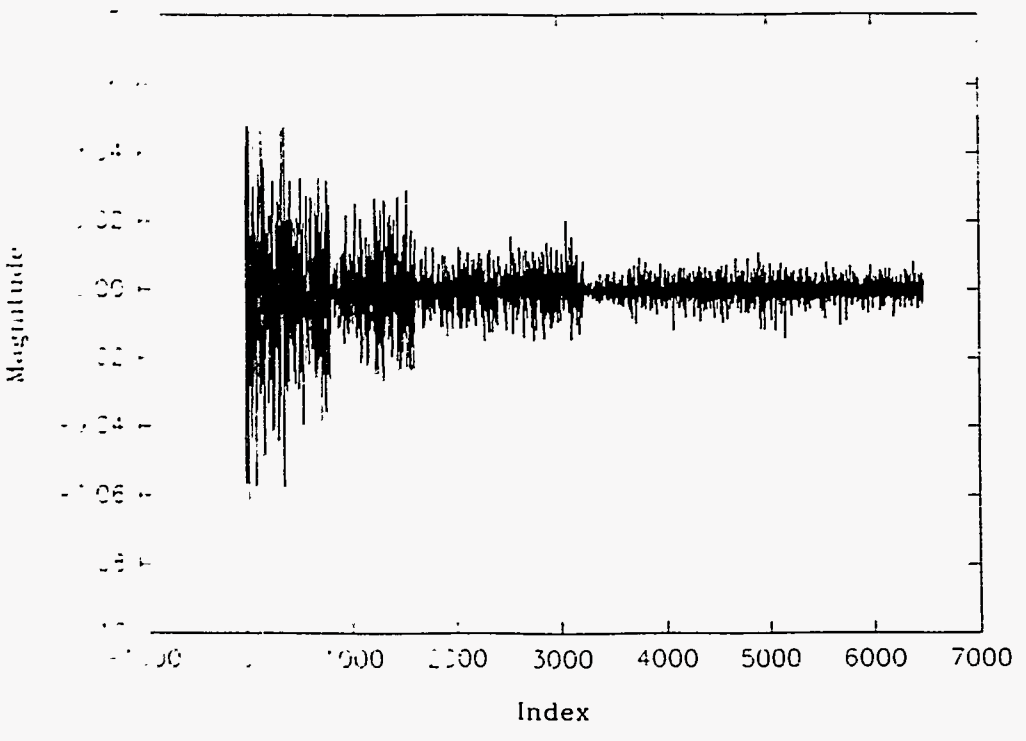

Figure 26 - Result of Walsh Transform Analysis of Fractal Waveform

leading to spiral deposition patterns.

Speculations could be offered about the effect of using current waveforms based on fractal time series. For example, it is possible that, with appropriate choice of parameters, the resonant hydrodynamic structures that occur in plating systems (such as spirals) might be damped[10] by applying fractal-time-series boundary conditions. Also, if there is a structural signature from the fractal waveform remaining in the electroformed deposit, these deposits might have unusual absorption behavior for specific wavelengths of electromagnetic radiation

Summary

This study demonstrated that by changing the way that anodic (deplating) current is distributed through a pulsed waveform, especially using a fractal design paradigm, control over the morphology of plated material can be increased. These results were encouraging enough to prompt the filing of a patent application with the U. S. Patent and Trademark Office, on the use of fractally-structured control variables. A U S patent[11] was granted on this process in January of this year. The means of carrying out investigations on this technology are relatively simple and available to most organizations working in the pulsed-plating field. There is no bar to research activities in this area; with respect to commercial applications, licensing arrangements may be pursued with the legal staff of Lockheed Martin Energy Systems, Inc.

Power Supply Survey

A set of specifications for a power supply that would be able to produce the kind of waveforms needed for industrial/commercial application of the fractal waveform technology (+/- 1000A, 100V at an adequate duty cycle, with adequate rise time and capability to accept programming of the type needed) was circulated to 26 power supply vendors listed in a register of companies. We requested information from each about whether they could supply such a system; we received three affirmative responses. This survey was completed in 1992, and it is possible that additional capability might be available now.

Conclusion

The fractal-design paradigm should be pursued as a way of optimizing microstructure and surface morphology of electroformed material.

Acknowledgements

The authors would like to thank: Bruce D. Hale for assisting in performance of plating experiments; Anna G. Dobbins for photographic and metallographic support; Clyde M. Davenport, J. T. Greer, and Leonard J. Gray for helpful discussions; and Lockheed Martin Energy Systems, Inc., Lockheed Martin Energy Research, and the U. S. Department of Energy for support of this work.

References

1. J. C. Puippe and F. Leaman, Eds., *Theory and Practice of Pulse Plating*, American Electroplaters and Surface Finishers Society, Orlando, FL (1986)

2. H. J. Weisner, *Lead*, Report UCRL-50895, Lawrence Radiation Laboratory, University of California, Livermore (1970)

3. D. J. Roha, *The Modeling of Additive Effects upon Electrodeposition Kinetics and Surface Leveling*, PhD dissertation from Case Western Reserve University, Cleveland, OH (1989)

4. HEATING is available from the Radiation Shielding Information Center, Building 6025 MS 6362, ORNL, Box 2008, Oak Ridge, TN 37831-6362.

5. K. W. Childs, *HEATING 7.2 User's Manual*, Report ORNL/TM-12262, Oak Ridge National Laboratory, Oak Ridge, TN, February, 1993 (available from Office of Scientific and Technical Information, Box 62, Oak Ridge, TN 37831).

6. J. R. Kirkpatrick, *Fluid Flow Effects on Electroplating*, Report K/CSD/TM-88, Martin Marietta Energy Systems, Inc., Oak Ridge, TN (1990); also *Addendum to Fluid Flow Effects on Electroplating*, Report K/CSD/TM-88 ADDENDUM

7. J. S. Bullock, G. Giles, and L. J. Gray, "Simulation of an Electrochemical Plating Process", in *Topics in Boundary Element Research, Vol.7*, Springer-Verlag, Berlin (1990)

8. K. G. Beauchamp, *Applications of Walsh and Related Functions*, Academic Press, Orlando, FL (1984)

9 Y Sugie, T Motooka and S Fujii, *Zairyo*, 40, 455, pp 1003-1008 (Aug. 1991) (English translation is Oak Ridge National Laboratory Report Y/OLS-92/31)

10. "Beating a Fractal Drum", *Science*, Dec. 13, 1991, p 1593

11. J S Bullock and R. L. Lawson, U S Patent 5,486,280 (1996)

Distribution

Oak Ridge National Laboratory

J. R. Kirkpatrick

Oak Ridge Y-12 Plant

J. S. Bullock (2)
R. L. Lawson
A. K. Lee/DOE-OSTI (2)
R. D. Mikkola
W. E. Smith/M. J. O'Hara
Y-12 Central Files